1985ApJ...290..449S

THE ASTROPHYSICAL JOURNAL, 290:449–461, 1985 March 15
© 1985. The American Astronomical Society. All rights reserved. Printed in U.S.A.

SPATIAL VARIATIONS IN THE PHYSICAL CONDITIONS IN THE GIANT EXTRAGALACTIC H II REGION NGC 5471

EVAN D. SKILLMAN[1,2]
Astronomy Department, University of Washington
Received 1984 May 10; accepted 1984 October 1

ABSTRACT

The giant extragalactic H II region NGC 5471 in M101 has been observed with high spatial resolution at both optical and radio wavelengths. Variations are found in reddening, gas temperature, ionic abundances, and stellar populations. Evidence for a supernova remnant has been discovered. These results are discussed with regard to previous research on extragalactic H II regions. An upper limit on the presence of Wolf-Rayet stars in NGC 5471 implies that the winds of Wolf-Rayet stars are not solely responsible for the large velocity dispersions in the ionized gas. It is shown that the presence of a supernova may be difficult to detect using standard methods; however, a supernova remnant will alter the results of estimates of physical conditions and chemical abundances.

Subject headings: galaxies: individual — nebulae: H II regions — nebulae: individual — nebulae: supernova remnants

I. INTRODUCTION

In a recent review paper, Rosa (1983) discussed the importance of the study of giant extragalactic H II regions (GEHR) and the areas of GEHR research needing further improvement. One of the main concerns affecting the interpretation of GEHR observations is the problem of spatial resolution. GEHRs are recognized to exhibit a core halo structure (Sandage and Tammann 1974*a*), and the cores frequently show detailed structure (Kennicutt 1979). Thus, observations of the light output of a GEHR will most certainly represent an intensity-weighted average of light produced in a variety of conditions. Since GEHRs at different distances are observed with the same size aperture, the relative contributions from various components of the nebulae will differ. Any correlations or comparisons of derived physical properties may be subject to biases.

The effects of finite aperture size and resolution are important at both radio and optical wavelengths. Optical observations of GEHR have been made from distances of 0.05–350 Mpc (Rosa 1983) where 1″ covers 0.24–1700 pc. Often spectrophotometric observations of GEHR are made with rectangular entrance apertures, ranging up to 10″ in length, in which spatial resolution is sacrificed in order to maximize both spectral resolution and light gathering. The resolution of radio observations has only recently matched that of optical observations. To date, most radio observations of GEHRs are unresolved, global values (Israel and Kennicutt 1980). Thus, optical/radio comparisons are frequently confined to comparisons of global radio values with optical observations made with apertures covering only a small fraction of the nebula.

This paper is a detailed study of a single relatively nearby GEHR, NGC 5471, in which it is possible to resolve spatially distinct components. Comparison of observations made in different parts of the nebula will allow an investigation of variations in reddening, the derived temperatures and densities, and the derived abundances. NGC 5471 is the most luminous H II complex in the giant spiral galaxy M101 (Seyfert 1940). At a distance of 7.2 Mpc (Sandage and Tammann 1974*b*) 1″ corresponds to 35 pc. NGC 5471 has a halo diameter of 30″ and a core diameter of 13″ (Sandage and Tammann 1974*a*), thus allowing the study of substructures using small aperture spectrophotometry, optical imaging, and VLA radio imaging. The purpose of this study is twofold: to probe the fine structure and to ascertain the point-to-point fluctuations of physical conditions within the GEHR.

Sections II, III, and IV will describe the optical imaging, optical spectroscopy, and radio imaging observations. In § V, an analysis and interpretation of the data is presented, with a concentration on the problems of reddening and extinction, ionic and total abundances, and the presence of supernova remnants and Wolf-Rayet stars. The relationship of the results of § V to current problems in GEHR research is discussed in § VI, and § VII contains a list of conclusions.

II. OPTICAL IMAGING

Narrow-band optical images were obtained with the video camera (Butcher and Oemler 1978) and the 2.1 m telescope of the Kitt Peak National Observatory on 1982 April 2. The seeing was measured to be 2.″0 (FWHM) for all frames. The format of the video camera allows 0.″56 per pixel, and the field of view (256 × 256 pixels) is much larger than the nebula. Table 1 lists the filter characteristics and exposure times for the observations. There is probably a small amount of contamination of the λ6563 image by the λ6548 line of [N II] (the λ6584 line is removed from the bandpass by a 5 Å redshift of NGC 5471), but from spectrophotometry (§ III) this is seen to be negligible (less than 1%). The standard KPNO reduction programs were used to correct for low and high frequency spatial sensitivity variations and geometrical distortions in the detector. Positions of intensity maxima were measured using a two-dimensional point-spread function fitting available within the RICHFLD photometry code of the IPPS (Tody 1980). All exposures were shifted to a common grid using cubic spline

[1] Visiting Astronomer at the Kitt Peak National Observatory (KPNO), which is operated by the Association of Universities for Research in Astronomy, Inc., under contract with the National Science Foundation.

[2] Visiting Astronomer at the National Radio Astronomy Observatory (NRAO), which is operated by Associated Universities, Inc., under contract with the National Science Foundation.

© American Astronomical Society • Provided by the NASA Astrophysics Data System

1985ApJ...290..449S

TABLE 1

TELESCOPE PARAMETERS

Observation Frame		Filter Characteristics λ (Å)	Δλ (Å)	Integration Time (minutes)
Hα	ON	6563	20	13.7
	OFF	6400	100	6.8
Hβ	ON	4861	30	13.7
	OFF	4693	138	6.8
λ5007	ON	5007	16	13.7
	OFF	5300	128	6.8

interpolation. The alignment error was judged to be less than 0″.25, or one-eighth of the seeing disk. To measure this error, arbitrary frames were shifted by a fraction of a pixel. When a ratio map was made from the division of a shifted image and an unshifted image, systematic asymmetries were detected for shifts less than 0.5 pixels. A sky level was determined from several measurements and subtracted from each image. The ON and OFF frames were then calibrated for relative throughput from exposures of KPNO standard stars, and the OFF frames were scaled accordingly and subtracted from the ON frames. Inherent in this correction method is the assumption of a flat continuum between the ON and OFF filters in the NGC 5471 exposures. This is not necessarily the case, but the equivalent width of the three lines observed is so large that the uncertainty involved in this subtraction is usually less than 1%.

In order to increase the signal-to-noise ratio in the fainter regions of the images, the images were convolved with a two-dimensional Gaussian. By choosing a FWHM for the smoothing function of less than the size of the seeing disk, only a small loss in spatial resolution is incurred. Figures 1*a*, 1*b*, and 1*c* show contour maps of the smoothed Hα, Hβ, and λ5007 images. The core of the region is dominated by several intensity peaks. Following Skillman and Balick (1984), these peaks will be referred to as nuclei. The positions of the various nuclei have been marked on the Hα plot. Figure 2*a* is a contour map of the optical continuum near Hβ.

A quick inspection reveals that the Hα and Hβ images are nearly identical. The only major difference occurs in the southwest corner where Hβ appears weaker. The continuum at nucleus D is much stronger relative to the nebular emission than at the other nuclear positions. This is also noted in the spectrophotometry (§ III) as a smaller equivalent width of the Hβ line.

The images were then divided to show variations in the line strength ratios across the nebulae. These images were scaled to true flux ratios by comparing the total light in the line images to fluxes obtained from large-aperture spectrophotometry obtained with the KPNO IRS (see § III). The ratio images are displayed as contour maps with solid and dashed contours at positive and negative percentages of the ratios determined

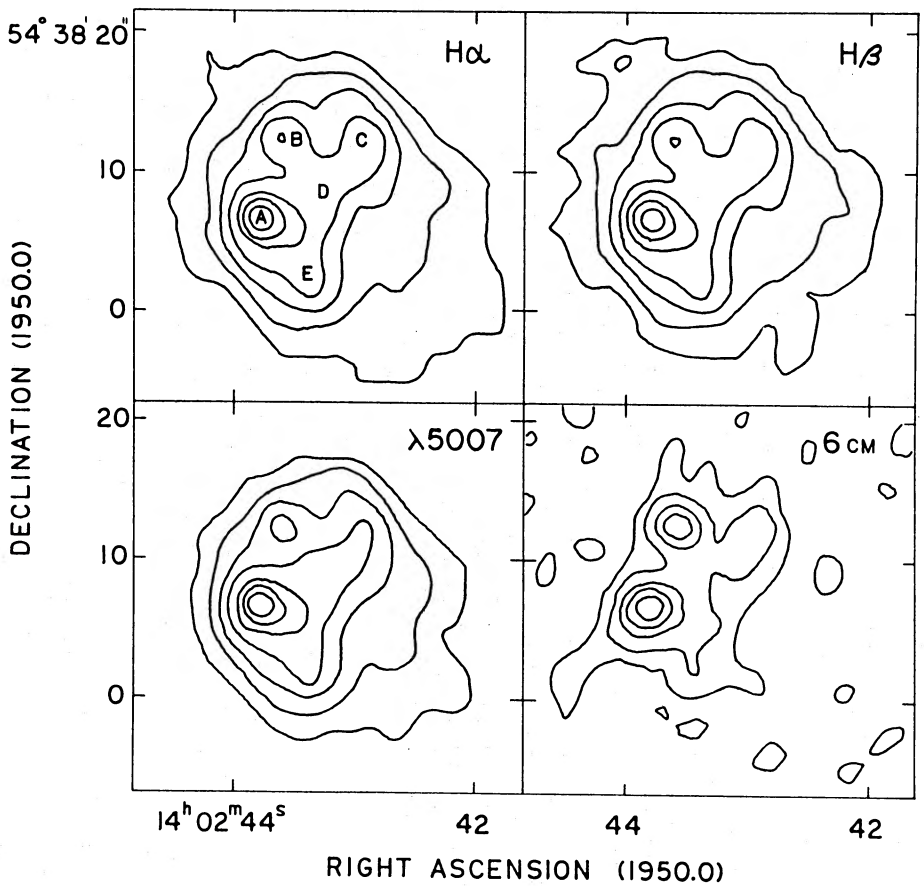

FIG. 1.—Contour maps of images of NGC 5471 in the light of (*a*) Hα λ6563; (*b*) Hβ λ4861; (*c*) [O III] λ5007, and (*d*) radio continuum λ = 6 cm. The contour levels are at 80%, 60%, 40%, 20%, 10%, 5%, and 2.5% of the peak, except in (*d*) where the 5% and 2.5% contour levels have been omitted. The peak surface brightness in the optical images are 6.7, 2.4, and 19.7 × 10^{-14} ergs s^{-1} cm^{-2} $arcsec^{-2}$ for the Hα, Hβ, and λ5007 images, respectively.

© American Astronomical Society • Provided by the NASA Astrophysics Data System

1985ApJ...290..449S

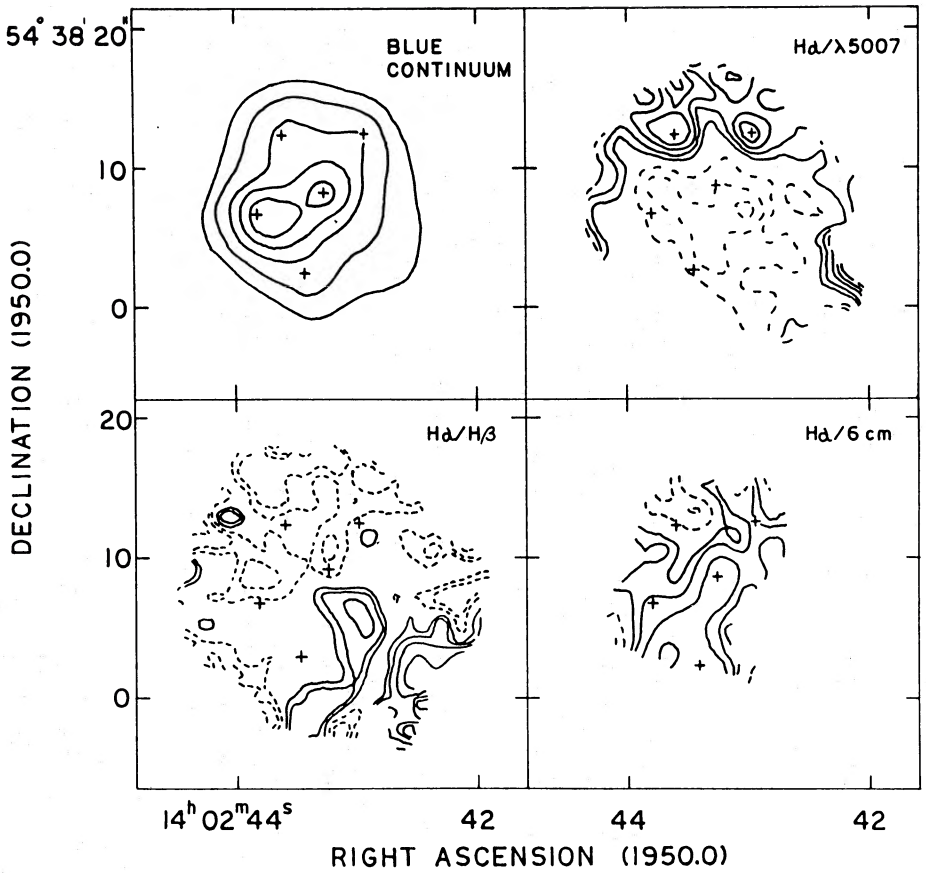

FIG. 2.—(*a*) Image in the blue continuum at 4700 Å. Contour levels are at 80%, 60%, 40%, 20%, and 10% of peak. The positions of nuclei A, B, C, D, and E are marked. (*b*) The λ6563/λ5007 ratio map. Positive contours are solid lines, negative contours are dashed. Contour levels are at 10% increments with regard to the image mean as derived from large-aperture spectrophotometry (see text). (*c*) The λ6563/λ4861 ratio map. Contour levels same as (*b*) except at 5% increments. (*d*) The λ6563/λ = 6 cm ratio map. Contour levels are at 20% increments.

from the large-aperture spectrophotometry. Figures 2*b* and 2*c* show the Hα/Hβ ratio and Hα/λ5007 ratio presented in this manner.

The Hα/Hβ ratio map shows that the variations in the ratio are, in general, small (usually less than 5%). There is evidence of obscuration in the southwest quadrant, probably due to a foreground cloud. The Hα/λ5007 ratio map shows two trends. First, there is a strong radial gradient for this ratio. Second, the B and C nuclei show anomalously large values of Hα/λ5007. From the results of the Hα/Hβ map it is obvious that the variations in the Hα/[O III] map cannot be a result of reddening variations.

III. SPECTROPHOTOMETRY

a) Description of Observations

NGC 5471 was observed with the KPNO 2.1 m and 0.9 m telescopes and the Mount Lemmon 1.5 m telescope at a number of positions. The telescope parameters are listed in Table 2. The positions of the small-aperture observations were determined from the narrow-band optical imaging described above. The large-aperture observation was centered on the core of the region. In all cases simultaneous observations of the sky enabled the sky contribution to be subtracted automatically. For all observations, the seeing was better than 3″. The positioning of the small-aperture observations is judged to be repeatable to within 1″. The sizes of the small apertures and the limit of the observations to small hour angles (less than 2 hr for all observations, less than 1 hr for the IIDS observations) precludes the loss of the blue light due to differential atmospheric extinction (Filippenko 1982). For all observations, KPNO standard stars were observed, enabling the conversion from instrumental counts to absolute fluxes. The calibration of the IIDS measurements, for which four or five standard stars were observed each night, are described here. These spectra were

TABLE 2

TELESCOPE PARAMETERS FOR THE OPTICAL SPECTROPHOTOMETRY

Telescope	Instrument	Aperture	Resolution (Å)	Wavelength Coverage	Positions
Mt. Lemmon 1.5 m	IDS	4.″7	12	4000–6800	A, B, C, D
KPNO 2.1 m	IIDS	4.2	8	3400–5200	A, B, C, D
				5600–7400	A, B, C
KPNO 0.9 m	IRS	22.0	13	3600–7200	core

© American Astronomical Society • Provided by the NASA Astrophysics Data System

1985ApJ...290..449S

reduced using the code available on the KPNO IPPS. After inspection of the calibration curve for each individual star, all of the standard star observations for a single night were used to solve for the overall instrumental calibration. The end-to-end rms deviation for each star in each aperture was typically 5%, so the uncertainty in the end-to-end calibration of the IIDS spectra should be less than 5%.

Line strengths were measured with a Gaussian fitting routine. In those cases where lines were blended, or nearby lines affected the estimation of the continuum, simultaneous solutions for a number of lines were calculated. This method yielded error estimates which, in turn, allow a comparison of the relative uncertainty in line strength measurements. It should be emphasized that these errors are not true errors in the sense of photon-counting statistics. However, they do include the uncertainty of the placement of the continuum. This can have an appreciable effect on the determined strengths of faint lines, especially in the blue end of the spectrum where lines are crowded.

b) *The Reddening Correction*

Typically, corrections for reddening are made by comparing the observed intensity ratios of the Balmer emission lines to the ratios predicted theoretically. This procedure has acknowledged uncertainties for GEHR (Tully *et al.* 1981), and it is typical for the logarithmic reddening correction at Hβ, c(Hβ), to increase with decreasing wavelength of the Balmer series lines. The values for c(Hβ) were calculated for the Hx/Hβ ratio for $x = \alpha$, γ, δ, and 9 and an equivalent width of underlying absorption of 0, 1, 2, and 3 Å. For all of the spectra, the most suitable agreement was found for 2 Å of underlying absorption, as in previous studies of GEHR (e.g., Shields and Searle 1978). The values of c(Hβ) determined from the calculations of both cases with no underlying absorption and 2 Å equivalent width of underlying absorption are presented in Table 3. The latter values of c(Hβ) were chosen to make the reddening corrections. The formal errors for c(Hβ) derived from the uncertainty in the line strength ratios were uncomfortably small, so 0.05 was adopted for the uncertainty in c(Hβ) for all further calculations.

For the sake of comparison, the values of $f(\lambda)$ used were those listed by Rayo, Peimbert, and Torres-Peimbert (1982; hereafter RPT) as derived from the normal galactic extinction law (Whitford 1958). The recommendation of McCall (1982) to use the mean galactic reddening law determined by Schild (1977) is acknowledged; however, it is felt that the value of direct comparison with published data is more important for this study. Table 4 lists the dereddened line strengths, the values of c(Hβ) used, and the equivalent width of Hβ for all of the observations. The errors quoted represent the propagation of the errors associated with the line strength measurements and the uncertainty in c(Hβ). Systematic errors for the small-aperture measurements can be best judged by comparing the KPNO values to the Mount Lemmon values. For the KPNO IIDS observations, c(Hβ) was determined from the blue scans and used for both the blue and the red scans. The intensities of the red scans were normalized by an iterative method of solving for the electron temperature from the [O III] lines and then fixing the Hα/Hβ ratio to be in agreement with the theoretical value (Brocklehurst 1971).

c) *Determination of Physical Parameters*

Several physical parameters are derived from the optical spectra and listed in Table 4. Temperatures were calculated from the temperature sensitive [O III] line ratio (λ5007 + λ4959/λ4363) following Seaton (1975). There is quite good agreement between the KPNO and Mount Lemmon observations. The four nuclei observed show a modest range in temperature, with nucleus B having the highest temperature. In nucleus B, the relatively strong presence of the [O I] and [S II] emission indicates that collisional ionization plays a significant role there.

Small variations are noted in the density-dependent [S II] λ6716/λ6731 line ratio. Approximate electron densities have been calculated following Pradhan (1978). The uncertainties show the range of values resulting from the uncertainty in the temperature estimate. In all cases, the densities fall within the range 100–1000 cm^{-3}, typical of GEHR. There is good agreement between the KPNO and Mount Lemmon data, except

TABLE 3

VALUES FOR c(Hβ)

	KPNO					MOUNT LEMMON			
RATIO	A	B	C	D	IRS	A	B	C	D
No Underlying Absorption									
Hα/Hβ.....	...	...	...	...	0.04	0.17	0.19	0.25	−0.01
	...	...	...	...	(0.02)	(0.01)	(0.01)	(0.01)	(0.01)
Hγ/Hβ.....	0.56	0.57	0.47	0.28	0.28	0.47	0.21	0.48	−0.01
	(0.02)	(0.02)	(0.03)	(0.03)	(0.06)	(0.03)	(0.04)	(0.03)	(0.04)
Hδ/Hβ.....	0.66	0.64	0.34	0.55	0.43	0.19	0.31	0.05	0.11
	(0.03)	(0.03)	(0.03)	(0.05)	(0.08)	(0.05)	(0.07)	(0.07)	(0.10)
H9/Hβ.....	0.93	0.99	0.93	1.54	0.70	...	...	...	...
	(0.07)	(0.10)	(0.12)	(0.21)	(0.20)	...	...	...	...
2 Å E.W. Underlying Absorption									
Hα/Hβ.....	...	...	...	...	0.03	0.16	0.18	0.24	−0.02
	...	...	...	...	(0.02)	(0.01)	(0.01)	(0.01)	(0.01)
Hγ/Hβ.....	0.52	0.51	0.42	0.17	0.21	0.39	0.15	0.40	−0.10
	(0.02)	(0.02)	(0.03)	(0.03)	(0.07)	(0.03)	(0.04)	(0.03)	(0.04)
Hδ/Hβ.....	0.58	0.52	0.23	0.29	0.32	0.07	0.20	−0.07	−0.06
	(0.02)	(0.03)	(0.03)	(0.05)	(0.07)	(0.05)	(0.06)	(0.06)	(0.09)
H9/Hβ.....	0.55	0.47	0.37	0.27	0.20	...	...	...	...
	(0.05)	(0.07)	(0.09)	(0.09)	(0.015)	...	...	...	...

© American Astronomical Society • Provided by the NASA Astrophysics Data System

1985ApJ...290..449S

TABLE 4

LINE FLUXES AND PHYSICAL PARAMETERS

Line	Id	A		B		C		D		IRS		AL		BL		CL		DL	
3727	[O II]	1.32	.04	3.00	.11	2.04	.08	1.26	.05	1.56	.06	...	...	...	...	...	...	1.61	.08
3750	H 12	.021	.003	...	...	.013	.006	...	...	...	...	...	...	...	...	...	...	...	...
3770	H 11	.026	.003	.018	.004	.017	.004	.012	.004	...	...	...	...	...	...	...	...	...	...
3798	H 10	.037	.003	.038	.004	.030	.004	.034	.005	.023	.007	...	...	...	...	...	...	...	...
3835	H 9	.057	.003	.054	.004	.050	.004	.031	.004	.049	.007	...	...	...	...	...	...	...	...
3868	[Ne III]	.56	.02	.37	.01	.40	.01	.49	.02	.38	.02	...	...	...	...	...	...	.56	.04
3889	H 8 + He I	.20	.01	.19	.01	.19	.01	.17	.01	.19	.01	...	...	...	...	...	...	.13	.02
3967	H 7 + [Ne III]	.34	.01	.28	.01	.28	.01	.29	.01	.28	.01	.31	.01	...	...	...	...	.22	.04
4026	He I	.016	.003	.011	.004	.016	.004	.015	.005	.009	.006	.013	.005	...	...	.031	.008	.018	.006
4069	[S II]	.009	.006	.038	.004	.021	.004	.019	.006	.024	.007	.027	.007	.028	.008	.079	.014	...	...
4076	[S II]	.010	.005	.017	.003	.009	.003	...	...	...	...	...	...	...	...	...	...	...	...
4102	H 6	.25	.01	.25	.01	.26	.01	.22	.01	.22	.01	.26	.01	.25	.01	.29	.01	.25	.01
4340	H 5	.47	.01	.46	.01	.45	.01	.46	.01	.44	.01	.43	.01	.47	.01	.44	.01	.47	.01
4363	[O III]	.10	.003	.062	.003	.054	.004	.072	.005	.081	.004	.090	.003	.084	.003	.056	.002	.064	.003
4471	He I	.036	.002	.032	.002	.032	.004	.033	.004	.034	.007	.038	.003	.038	.005	.040	.004	.030	.004
4658	[Fe III]	.006	.002	.009	.002	...	...	...	...	...	...	...	...	...	...	...	...	...	...
4686	He II	.011	.003	.013	.002	...	...	.013	.004	...	...	...	...	...	...	...	...	...	...
4712	[Ar IV] + He I	.016	.004	.005	.001	...	...	.011	.004	...	...	...	...	...	...	...	...	...	...
4861	H 4	1.00	.01	1.00	.01	1.00	.01	1.00	.01	1.00	.02	1.00	.01	1.00	.01	1.00	.01	1.00	.01
4959	[O III]	2.21	.02	1.25	.02	1.44	.01	1.97	.02	1.90	.08	2.26	.03	1.49	.03	1.57	.02	1.90	.03
5007	[O III]	6.97	.04	3.92	.02	4.60	.03	6.22	.04	5.64	.11	6.82	.06	4.71	.05	4.64	.03	5.95	.05
5876	He I	.087	.005	.093	.004	.093	.004	...	...	.11	.01	.092	.003	.085	.003	.086	.003	.093	.004
6300	[O I]	.033	.003	.14	.005	.039	.004	...	...	.052	.004	.022	.001	.10	.01	.040	.002	.013	.001
6312	[S III]	.011	.002	.017	.002	.010	.002	...	...	.022	.004	.013	.001	.005	.002	.013	.001	.016	.001
6563	H 3	2.80	.11	2.79	.11	2.81	.11	...	...	2.73	.11	2.78	.11	2.79	.11	2.81	.11	2.80	.11
6584	[N II]	.061	.009	.13	.01	.16	.01	...	...	.17	.01	.077	.010	.16	.01	.17	.01	.091	.009
6678	He I	.021	.003	.024	.004	.020	.003	...	...	.019	.005	.021	.002	.022	.003	.026	.003	.029	.003
6716	[S II]	.081	.005	.26	.01	.15	.01	...	...	.11	.006	.082	.004	.24	.01	.14	.01	.091	.005
6731	[S II]	.060	.003	.22	.01	.12	.01	...	...	.10	.006	.071	.003	.19	.01	.11	.01	.073	.004
7065	He I	.024	.008	.016	.006	.036	.013	...	...	...	...	.021	.002	.027	.003	.014	.003	...	...
7136	[Ar III]	.051	.007	.040	.006	.055	.011	...	...	...	...	...	...	.063	.004	.046	.003	...	...
7281	He I	.006	.006	...	...	...	...	...	...	...	...	...	...	...	...	...	...	...	...
7320	[O II]	...	...	.036	.006	...	...	...	...	...	...	...	...	...	...	...	...	...	...
7330	[O II]	...	...	.029	.005	...	...	...	...	...	...	...	...	...	...	...	...	...	...
c(HB)		.54	.05	.51	.05	.33	.05	.21	.05	.07	.05	.18	.05	.18	.05	.25	.05	.00	.05
EW(HB)		297	...	238	...	245	...	105	...	217	...	244	...	223	...	206	...	139	...
T(O III)		12,850	150	13,450	250	12,050	300	11,950	300	13,000	300	12,500	150	14,150	350	12,050	200	11,650	200
ne(S II)		100	50	400	200	300	200	...	...	600	200	400	200	400	200	300	200	350	200
Teff		42,500	...	39,500	...	37,500	...	39,000	...	40,000	...	...	...	...	...	...	...	40,000	...

for the significant discrepancy between the two values for position A. The [O II] and [S II] lines from nucleus B are sufficiently strong that the ratio of the transauroral to nebular lines can be used to determine the temperature at that position. Assuming an electron density of 400 ± 200 cm^{-3}, the [S II] lines yield $11{,}100 \pm 1500$ K, and the [O II] lines yield 9700 ± 1200 K. Stellar effective temperatures have been estimated following the method of Kunth and Sargent (1983) (KS). Again, there is good agreement between the Mount Lemmon and KPNO data, except for nucleus B where the difference in the [O III] temperature has led to a significant discrepancy. It should be noted here that the reduced equivalent width of Hβ for nucleus D is not reflected by a smaller effective temperature estimate for this position. This would imply that the equivalent width of the Hβ line may not be a reliable estimator of the temperature of the exciting stars as suggested by Shields and Tinsley (1976).

By comparing the large-aperture IRS observation with the smaller aperture observations, one can investigate the possible effects of a loss of spatial resolution that would occur when looking at a more distant GEHR. It is surprising that the temperature derived for the large-aperture observation is so high. This is higher than a sum of the light from the four small-aperture positions would yield. It is possible that this could be an instrumental effect. The IRS affords the lowest spectral resolution of the three spectrophotometers used, and this may affect the ability to separate the λ4363 line from the relatively strong λ4340 line. A second significant result is the large difference in the value of c(Hβ). The large-aperture observation indicates a lower value of reddening.

Figure 3 shows the four IIDS spectra in the region between λ4400 and λ4850. There is no evidence of the broad lines of N III, N V, C III, or C IV associated with Wolf-Rayet stars. He II λ4686 is detected, but is too weak for reliable measurements of line width. D'Odorico, Rosa, and Wampler (1983) used a $2'' \times 4''$ aperture to obtain a spectrum of NGC 5471 for the explicit purpose of looking for evidence of Wolf-Rayet stars. The agreement between the spectrum of nucleus A presented here and their spectrum of NGC 5471 is quite good. An interesting feature to note in Figure 3 is the detection of the [Mg I] lines at 4562 and 4571 Å in nucleus B.

IV. RADIO IMAGING

On 1981 July 10, VLA observations of NGC 5471 were made at 1420 MHz in the spectral line mode. An additional continuum observation was made at 4885 MHz on 1981 October 26. The observing parameters and flux measurements for both of these observations are listed in Table 5.

Figure 4 shows the $\lambda = 21$ cm and $\lambda = 6$ cm continuum maps produced from these observations. A 40 kilowavelength

© American Astronomical Society • Provided by the NASA Astrophysics Data System

1985ApJ...290..449S

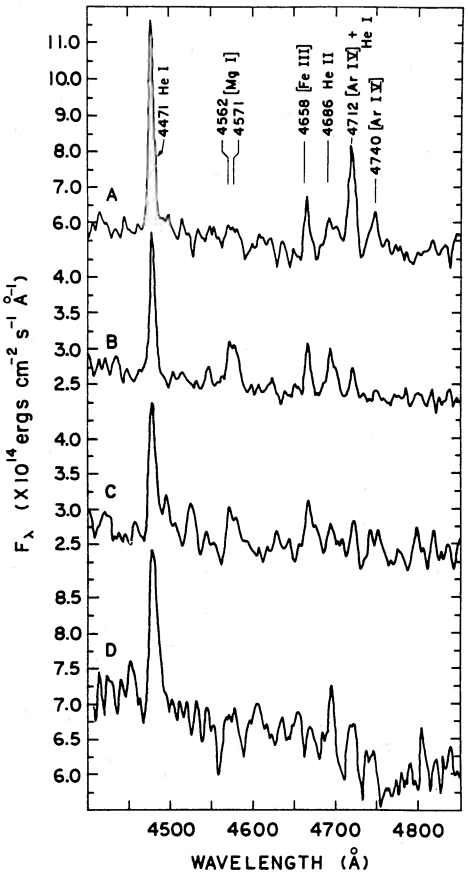

FIG. 3.—The IIDA spectra for the nuclei A, B, C, and D from 4400 to 4850 Å. The lines of He I λ4471, Mg I λ4562 and λ4571, [Fe III] λ4658, He II λ4686, He I + [Ar IV] λ4712, and [Ar IV] λ4740 are marked.

taper has been applied to the data, resulting in a beam size of ~4″. Nuclei A and B are clearly resolved at both frequencies, and nucleus C is detected. The $\lambda = 21$ cm observations are much noisier because of the smaller observing bandwidth. The flux measurements listed in Table 5 show that the spectral index, α, for nucleus B is definitely negative (where $S_\nu \propto \nu^\alpha$). Nucleus A has a flatter radio spectrum characteristic of a thermal source. From lower resolution radio continuum maps Israel, Goss, and Allen (1975) have made estimates of the electron density and mass of the ionized gas in the nuclei and core components of NGC 5471. Beyond the discovery of the nonthermal component, the present study is in close agreement with theirs. The improved resolution has led to smaller size linits on the nuclei, but not far from their assumed value of 3″.

The 90 minutes of C-configuration $\lambda = 6$ cm observations have been combined with 120 minutes of B-configuration $\lambda = 6$ cm observations to form a high signal-to-noise, high-resolution radio continuum map. The latter observations have been provided by Dr. R. Sramek of the National Radio Astronomy Observatory and Dr. D. Weedman of Pennsylvania State University. A map was produced from this combined data base and cleaned with a Gaussian restoring beam of 2.″5 FWHM. Figure 1*d* shows this $\lambda = 6$ cm map. Nuclei A, B, and C are all clearly detected. This map can be compared with the Hα map to investigate small-scale differences between the Hα/Hβ reddening index and the $H\alpha/\lambda = 6$ cm extinction index. Figure 2*d* shows the $H\alpha/\lambda = 6$ cm map. Nucleus B shows a relative excess of $\lambda = 6$ cm radiation. Nuclei D and E would

TABLE 5

A. TELESCOPE PARAMETERS FOR RADIO IMAGING

PARAMETER	FREQUENCY 1418.5 MHz	FREQUENCY 4885 MHz
VLA configuration	B	C
Number of antennae	25	27
Integration (minutes)	240	90
Total bandwidth (MHz)	6.25	50
Channel bandwidth (kHz/km s^{-1})	98/21	...
Number of channels	16	...

B. MEASUREMENTS

SOURCE	α	FLUX DENSITIES (mJy) 1418.5 MHz	FLUX DENSITIES (mJy) 4885 MHz
NGC 5471	−0.25 ± 0.1	13.7 ± 1.0	9.2 ± 1.0
Nucleus A	−0.3 ± 0.1	5.2 ± 0.8	3.7 ± 0.8
Nucleus B	−0.5 ± 0.1	4.4 ± 0.8	2.5 ± 0.5
Nucleus C	−0.1 ± 0.2	1.4 ± 0.6	1.4 ± 0.6

NOTE.—Radio map parameters are as follows:

MAP		MAP rms 1418.5 MHz	MAP rms 4885 MHz
Continuum	(4″ beam)	0.3	0.07
Line	(12″ beam)	4.0	...

Map rms is in millijanskys per beam.

appear to be relatively deficient in the radio continuum. Beyond the details noted above, no clear trends are evident.

Interferometric H I observations of NGC 5471 have previously been made by Viallefond, Allen, and Goss (1981; hereafter VAG) using the Westerbork Synthesis Radio Telescope. The observations presented here offer a better spatial resolution because of the larger baselines of the VLA. In Figure 5, the $\lambda = 21$ cm continuum map and maps of the three spectral line channels in which signal was detected are presented. All have been constructed with a strong taper resulting in a synthesized beam of 12″ FWHM. The largest concentration of H I appears to the northwest of the continuum peak. There is a suggestion of a local H I minimum at the position of the continuum maximum. The distribution of H I around the continuum maximum is definitely not symmetric. The most H I deficient region is to the southwest. The total H I content detected in the three line channels is $60 \pm 15 \times 10^6\ M_\odot$, comparing favorably with the $86 \pm 14 \times 10^6\ M_\odot$ reported in VAG. Given the lack of short baselines in the B-array, these observations will not be sensitive to extended emission on the order of 1′ or larger. Since 70% of the H I was detected at this higher resolution, it can be concluded that most of the H I is concentrated in the clouds detected. A cylindrical model for the main concentration of H I yields an average density of 3.4 atoms cm^{-3}, which, considering the uncertainty of the model, is in good agreement with the value of 1.2 atoms cm^{-3} derived in VAG.

V. ANALYSIS AND INTERPRETATION

a) Reddening and Extinction

Israel and Kennicutt (1980) have investigated the extinction of extragalactic H II regions as derived from the Balmer decrement and a comparison of Hα flux and radio continuum flux. Assuming a conventional extinction law ($A_v = 3E[B - V]$), the optical/radio extinction measure shows greater extinction

© American Astronomical Society • Provided by the NASA Astrophysics Data System

1985ApJ...290..449S

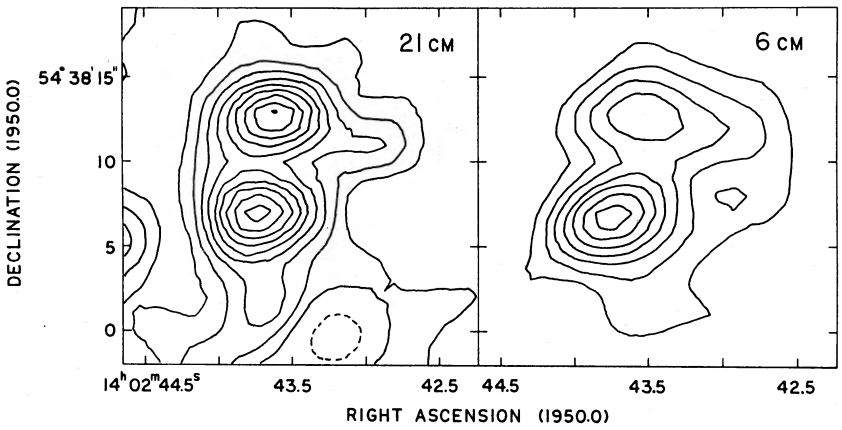

FIG. 4.—Contour maps of radio continuum images at $\lambda = 6$ cm and $\lambda = 21$ cm. Contour levels are at 0.3 mJy

than the optical measurement for all regions observed. For NGC 5471 they find an excess in A_v of 1.3 mag. NGC 5471 is at a galactic latitude of 60° and therefore galactic reddening can be assumed to be zero (Sandage 1973; and Sandage and Tammann 1974*b*). This assumption is further supported by the evidence compiled by Lequeux *et al.* (1981), and especially the ultraviolet observations of Rosa (1980).

Israel and Kennicutt consider both internal and foreground dust as explanations for the discrepancies between the two extinction measures; however, their data do not allow them to distinguish between the two. In the case of foreground dust, one would expect random variations in the Hα/Hβ ratio since the distribution of foreground dust should not be correlated to any structure within the H II region. Since reddening by internal dust increases as a function of light path length until the dust becomes optically thick at the Balmer lines, reddening by internal dust might be strongest in the brightest/densest regions of the nebula. There is evidence for both types of reddening in the Hα/Hβ ratio map. The lane of increased Hα/Hβ ratio in the southwest and the entire southwest corner of the nebula would be explained most easily by foreground clouds. (If these clouds are in M101 they are ~100 pc in diameter.) Certainly the presence of these two clouds cannot account for the entire discrepancy between the two extinction measures. However, the fact that the rest of the map looks relatively smooth does not rule out more foreground extinction. Many smaller cloudlets randomly distributed over the face of the region could produce significant extinction while remaining undetected by these seeing-limited observations.

The optical spectrophotometry shows evidence of increased reddening in the nuclei. Comparing the KPNO and the Mount Lemmon data, and constraining the comparisons to those

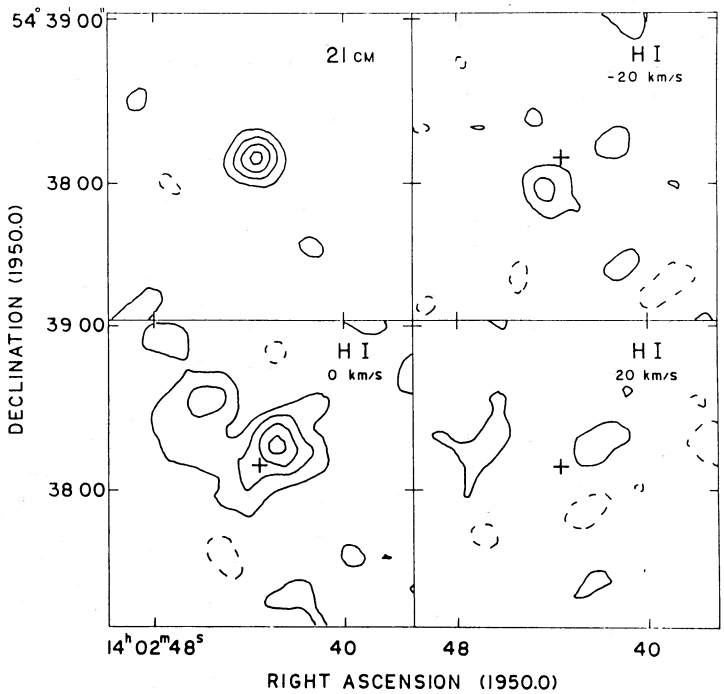

FIG. 5.—The $\lambda = 21$ cm observations reproduced with a 12″ beam. (*a*) The continuum image. Contour levels are at 2 mJy. (*b*)–(*d*) The H I channel maps at −20, 0, +20 km s^{-1} of the optical velocity of the ionized gas (280 km s^{-1}). Contour levels are at 5 mJy which translates to 7.9×10^{20} atoms cm^{-2}. The cross marks the center of the radio continuum emission.

© American Astronomical Society • Provided by the NASA Astrophysics Data System

1985ApJ...290..449S

Balmer lines in common, the reddening determined from the larger aperture observations is generally less than that determined from the smaller aperture observations. This trend can be further investigated by integrating over increasing areas in the video camera images. For each nucleus, measurements were made from concentric apertures. For the A, B, and C nuclei the Hα/Hβ ratio decreased by ~10% for the fluxes measured from 1″ diameter rings to the fluxes measured in 5″ diameter rings. For nucleus D the ratio first decreased and then increased. For nucleus E the ratio steadily increased with increasing radius up to 10% larger. Note that nuclei D and E are most likely affected by the foreground absorption lane already identified. The differences in the Hα/Hβ ratios between the large and small rings could not arise from seeing differences between the Hα and Hβ images because the outer rings are much larger than the seeing disk.

Although the differences measured here are small, under the assumption of an isothermal gas, they indicate that the reddening is greater in the centers of the nuclei than in the surrounding environment. This is taken as evidence of internal dust. In Figure 6, plots of the variation of the Hα/Hβ ratio as a function of right ascension at a constant declination are shown. The four slices cut through the positions of the nuclei. The value of these plots lies in the demonstration of the confidence of the ratios. It is clear that the variations observed are not smoothed noise features. The dust lane appears prominently. The increase of the Hα/Hβ ratio at the positions of nuclei B and C is clear.

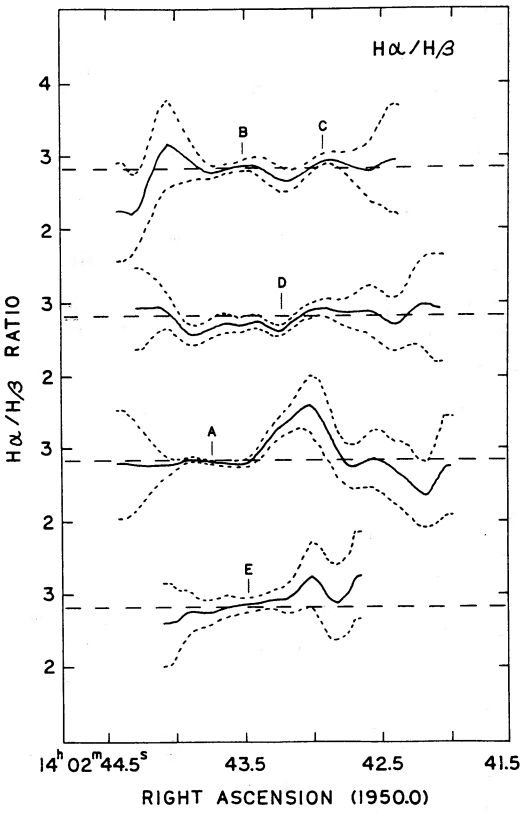

FIG. 6.—The Hα/Hβ ratio at a constant declination. The slices cut through B and C, D, A, and E nuclei. The dashed lines show 1 σ errors in the ratio. The errors were calculated by using the CORMS routine available in the NRAO AIPS system. The long dashes mark the theoretical case B value for 12,000 K.

Figure 6 also presents a distrubing problem. The horizontal dashed line indicates the theoretical value for the Hα/Hβ ratio at 12,000 K (Brocklehurst 1971). At some positions the ratio definitely drops below this value. This could be due to a miscalibration or possibly an increased gas temperature. The calibrating ratio derived from scaling the video camera ratio to the IRS ratio (2.88) is only slightly dependent on the position in the video camera images. Melnick (1979) obtained a measurement of the Hα/Hβ ratio with an aperture of 23″ and found an even smaller value (2.75). Adopting this result would increase the problem of "blueing." If the ratio is fixed by matching the map ratio at nuclei A, B, and C with the Mount Lemmon data, a larger value of the Hα/Hβ ratio for the total core is found (3.30). The internal consistency between the three nuclei is excellent, but the discrepancy with the IRS data and Melnick's observation is disturbing. There is evidence that the fluxes of strong emission lines measured with the IRS are subject to instrumental effects (Hayes and Massey 1984), but on the strength of the agreement with previous data, the IRS value is used.

b) Chemical Abundance Estimates

Relative abundances can be calculated from the optical spectroscopy. For these spectra, the [O III] and [S II] lines provide the only direct means for calculating the electron temperature and density. From the models of low abundance, high-excitation H II regions (Shields and Searle 1978; Stasinska 1980; French and Grandi 1981), it is clear that the electron temperature is lower in the O^+ zone than in the O^{++} zone. The best way to take temperature variations into consideration for abundance calculations is through modeling of the structure of the nebula (Osterbrock 1974). However, in practice, most abundance determinations follow the method of Peimbert and Costero (1969) wherein a mean squared temperature fluctuation is assumed. An alternate approach is offered by Kunth and Sargent (1983) in which estimates of oxygen abundance and stellar effective temperature are combined with model H II region calculations.

Since this work is more concerned with variations within the nebula than with absolute abundances, a one-zone model is used to interpret the spectra. Detailed models are not possible because there is insufficient information to model the volume fractions and temperatures of the different ionization zones. Calculations using the other methods were performed, but the necessary introduction of additional assumptions makes a direct comparison between spectra difficult to interpret. The comparison of methods is reported in a separate work (Skillman 1984).

The ionic abundances listed in Table 6 were calculated using an electron temperature derived from the [O III] lines, an electron density of 100 cm^{-3}, and emissivities computed by a five-level atom program originally written by Brugel (1980) and further developed by A. Raga at the University of Washington. The errors reported can come from uncertainty in the temperature estimates, which is primarily due to the uncertainty in the reddening correction, or from uncertainty in the line strength estimates. The larger of the two errors is always quoted. Those cases where the larger error is due to line strength uncertainty are marked with a colon.

The agreement between the KPNO and Mount Lemmon data is quite satisfactory and lends credence to both the observational technique and the error estimates. Table 6 reveals that the estimates of the O^{++} and Ne^{++} abundances at the posi-

© American Astronomical Society • Provided by the NASA Astrophysics Data System

1985ApJ...290..449S

TABLE 6

IONIC ABUNDANCES

Position	O^+/H^+ ($\times 10^5$)	O^{++}/H^+ ($\times 10^5$)	N^+/H^+ ($\times 10^7$)	Ne^{++}/H^+ ($\times 10^5$)	He^+/H^+ λ5876	He^+/H^+ λ4471	He^+/H^+ λ6678
A	1.66	9.45	5.71	2.03	0.068	0.076	0.058
	(0.07)	(0.31)	(0.83:)	(0.08)	(0.0035:)	(0.0039:)	(0.0086:)
AL	...	10.3	7.77	...	0.072	0.079	0.058
	...	(0.36)	(1.0:)	...	(0.0020:)	(0.0071:)	(0.0046:)
B	3.19	4.60	10.9	1.14	0.074	0.067	0.066
	(0.24)	(0.27)	(0.83:)	(0.08)	(0.0032:)	(0.0047:)	(0.010:)
BL	...	4.71	11.6	...	0.068	0.080	0.063
	...	(0.20)	(0.64:)	...	(0.0025:)	(0.0098:)	(0.0070:)
C	3.36	7.75	18.0	1.84	0.072	0.067	0.053
	(0.36)	(0.74)	(1.6:)	(0.19)	(0.0030:)	(0.0080:)	(0.0093:)
CL	...	7.93	18.9	...	0.066	0.085	0.071
	...	(0.45)	(1.2:)	...	(0.0024:)	(0.0091:)	(0.0083:)
D	2.13	10.7	...	2.34	...	0.068	...
	(0.21)	(0.94)	...	(0.23)	...	(0.0082:)	...
DL	3.06	11.3	11.1	2.96	0.071	0.063	0.078
	(0.23)	(0.71)	(1.1:)	(0.24:)	(0.0027:)	(0.0086:)	(0.0088:)
IRS	1.90	7.44	15.2	1.31	0.087	0.072	0.051
	(0.15)	(0.52)	(1.4:)	(0.11)	(0.0037:)	(0.014:)	(0.013:)

tion of nucleus B are significantly lower than at the other positions. As noted in § III, collisional ionization is important at this position, and the evidence for a supernova remnant at this position will be discussed in the next part of this section. The calculations for nucleus B do not try to correct for the presence of the shock heating detected there. These calculations are provided to demonstrate the potential effect of an undetected supernova remnant on standard abundance calculations. The next apparent trend in Table 6 is the large variation in the calculated N^+ abundances. Either there are real differences in the N^+ abundances, or there are large differences in the temperature of the N^+ zone. The difference in the N^+ abundance between nucleus A and C is roughly a factor of 3. If the temperature of the N^+ zone in nucleus C is assumed to be the temperature of the O^{++} zone (11,950 K), then requiring an equal N^+ abundance in nuclei A and C will allow a calculation of the temperature of the N^+ zone in nucleus A. This temperature is 8500 K. Given the internal consistency between the KPNO and Mount Lemmon line strength measurements, and the extreme conditions necessary to resolve the measurements under the assumption of uniform N^+ abundance, this is strong evidence for N^+ abundance variations within NGC 5471.

The variation in N^+ abundance is not a disturbing observation in itself. This is easily interpreted as a difference in the volume fraction of the N^+ zone for the area covered in the observations of the two nuclei. Considering the higher temperature for nucleus A, it would not be unreasonable to assume a larger fraction of nitrogen to be doubly ionized in nucleus A than in nucleus C.

What would be disturbing or interesting would be a variation in the total chemical abundance. The conversion of ionic abundances to total abundances is usually performed by assuming a two-zone model (e.g., Peimbert and Costero 1969) and calculating ionization correction factors. For nitrogen this calculation depends on the N^+/O^+ ratio. This ratio, along with the Ne^{++}/O^{++} ratio and the $(O^+ + O^{++})/H^+$ ratio, are presented in Table 7. Also included are the relative elemental nitrogen and neon abundances as derived using the ionization correction factors. The close agreement between the total oxygen abundances in nuclei A and C, and the large discrepancy in the N^+/O^+ ratio, imply a real nitrogen enhancement in nucleus C relative to nucleus A. Taken at face value, the relatively large value for N^+/O^+ for the IRS measurement would imply an even larger enhancement of nitrogen for the total core relative to the nuclei. However, it should be noted that the N^+/O^+ ratio is very sensitive to the reddening correction. If a value of $c(H\beta) = 0.5$ is used for dereddening the IRS spectrum, then the N^+/O^+ ratio decreases to 4.6 and becomes much closer to the values obtained from the small-aperture spectrophotometry. It should also be noted here that Rubin (1983) has shown that the opacity effects of elements heavier than helium can significantly alter the ionization structure of an H II region,

TABLE 7

IONIC ABUNDANCE RATIOS

Position	N^+/O^+ ($\times 10^2$)	Ne^{++}/O^{++}	$(O^+ + O^{++})/H^+$ ($\times 10^5$)	[N/H] ($\times 10^6$)	[Ne/H] ($\times 10^5$)
A	3.4 (0.5)	0.22 (0.01)	11.1 (0.3)	3.8 (0.6)	2.4 (0.1)
B	3.4 (0.4)	0.24 (0.02)	7.8 (0.4)	2.7 (0.3)	1.9 (0.2)
C	5.4 (0.8)	0.24 (0.03)	11.1 (0.8)	6.0 (1.0)	2.7 (0.4)
D	... ...	0.22 (0.03)	12.8 (0.9)	... ...	2.8 (0.4)
DL	3.6 (0.5)	0.26 (0.03)	14.4 (0.7)	5.2 (0.8)	3.7 (0.5)
IRS	8.7 (1.3)	0.18 (0.02)	9.3 (0.5)	8.1 (1.3)	1.7 (0.2)
IRS $c(H\beta) = 0.5$	4.6 (0.5)	0.23 (0.02)	7.9 (0.4)	3.6 (0.4)	1.8 (0.2)

© American Astronomical Society • Provided by the NASA Astrophysics Data System

1985ApJ...290..449S

casting doubt on the validity of ionization correction factors dependent on the coexistence of atomic species with similar ionization potentials.

c) *The Supernova Remnant*

In nucleus B there is evidence of collisional heating from the optical spectroscopy and evidence of nonthermal radio continuum emission. These observations are most easily accounted for by the presence of a supernova remnant. Here an attempt is made to calculate physical properties of the SNR.

A detailed analysis of the supernova remnant is dependent upon separating its spectrum from the surrounding nebulosity. This is all but impossible. It is possible, however, to assume that nucleus B would be comparable to the other nuclei if the SNR were absent. Investigating differences between the nuclei might yield information about the SNR.

The radio flux and spectral index of the SNR can be estimated by comparing the radio maps with the Hα map. Assuming the Hα/radio continuum flux ratio is a constant for all the thermal radio radiation, and that the Hα flux of nucleus B is all due to the thermal component, an estimate of the (minimum) nonthermal radio flux of the SNR at $\lambda = 6$ cm and $\lambda = 20$ cm can be made. This assumption produces a flux density for the nonthermal component of 2.1 ± 0.8 mJy at 1420 MHz and a spectral index of -0.7 ± 0.3. This would place the SNR among the most powerful known radio-emitting SNRs, with a radio luminosity at 1420 MHz 5 times more powerful than Cas A (Parker 1968; $\alpha = -0.77$), 9 times stronger than N132 D (Mathewson and Clarke 1973; $\alpha = -0.65$) and about one-third the strength of the SNR in NGC 4449 (Bignell and Seaquist 1983; $\alpha = -0.62$).

Divining the optical spectrum of the SNR is yet more treacherous. Table 8 shows the results of a comparison of the spectrum of nucleus B to the spectra of the other nuclei. The comparison was constructed by finding the difference between the line strengths of nucleus B and the other nuclei (normalized to Hβ) and then normalizing the difference by dividing by the comparison spectrum. In this way a list of enhanced or weakened lines is produced. The results for lines showing differences of more than 10% are listed in Table 8. In order to better interpret the results, the spectrum of the SNR in NGC 6822 (D'Odorico and Dopita 1983) is compared to the average spectrum of the H II regions Hubble V and Hubble X in NGC 6822 (Lequeux *et al.* 1979; Pagel, Edmunds, and Smith 1980). By using a comparison of H II regions and a SNR observed in a low-abundance environment, it is hoped that the abundance effects can be minimized. The chemical abundance has been shown to be the primary factor in determining the spectrum of an extragalactic SNR (Dopita *et al.* 1984).

The analysis of the optical spectrum of the SNR can start with a discussion of what is not present in the spectrum. There is no evidence for lines broader than the instrumental resolution (~ 300 km s^{-1}). If this SNR had a broad component only 1/10 as luminous as the SNR in NGC 4449, it would easily be detected in these measurements. The largest differences between the spectrum of nucleus B and the other nuclei are found at 6300 Å. This is as would be expected from the results of the NGC 6822 comparison. The [S II] lines also show the same trend of enhancement. The [N II] and [O II] lines are enhanced, but the difference is not as large. Of the three other nuclei, nucleus B is most like nucleus C. The gas in the local environment of the SNR is not being kept completely ionized by the surrounding stars as evidenced by emission from the neutral species of oxygen (6300 and 6363 Å) and magnesium (4562 and 4571Å). Further discussion of the optical emission of the SNR is difficult. It is safe to say that the derived optical spectrum is similar to that of a typical "old" SNR (e.g., the Cygnus Loop, Miller 1974; 30 Dor B; Danziger *et al.* 1981; Gilmozzi *et al.* 1983), by virtue of the strong [O I], [S II], and the detection of [Mg I].

Since it is possible for an SNR to remain undetected and yet subtly alter estimates of physical conditions and chemical compositions, it would be convenient to have a test for the presence of SNRs. Baldwin, Phillips, and Terlevich (1981; hereafter BPT) have discussed diagnostic diagrams for distinguishing the excitation mechanisms in extragalactic emission line objects. The different nuclei in NGC 5471 do not distinguish themselves in the $\langle E \rangle$ parameter developed in BPT. However, in a plot of λ6300/λ5007 versus λ3737/λ5007 (as suggested by Heckman 1980 for distinguishing Seyfert nuclei from LINERs) nucleus B does stand out as strongest of all positions observed in NGC 5471 in both ratios.

Figure 7 shows the plot of λ6300/λ5007 versus λ3727/λ5007. The nuclear and core spectra are indicated by letters. For comparison, the metal-poor galaxies of KS and the emission-line galaxies of French (1980) are also included. The regions of Seyfert nuclei and LINERs come from Heckman (1980), and the boundaries for planetary nebulae and H II regions are from BPT. The high-luminosity galaxies of French occupy the same region of the diagram as nucleus B. Despite the fact that the [O III] temperatures for the high-luminosity galaxies are lower than the temperature of nucleus B, there is evidence for supernova remnants in two of them. This is discussed in § VI.

d) *Wolf-Rayet Stars*

The presence of Wolf-Rayet (WR) stars in GEHR is of great interest. Smith and Weedman (1970, 1972) first noted the ubiquity of anomalously broad emission lines in GEHR and

TABLE 8

EVIDENCE OF SNR EMISSION

Line	IIDS (B − A)/A	IIDS (B − C)/C	IIDS/MT. L. (B − D)/D	NGC 6822 (SNR − H II)/H II
[O II] λ3727	+130%	+47%	+140%	+130%
[S II] λ4068+4076	+190%	+82%	+44%	...
[O III] λ4363	−38%	+14%	−13%	...
[O III] λ5007	−44%	−14%	−36%	−85%
[O I] λ6300	+320%	+250%	+670%	+6600%
[N II] λ6584	+110%	−18%	+76%	+270%
[S II] λ6716	+220%	+73%	+160%	+680%
[S II] λ6731	+270%	+89%	+160%	+1100%

© American Astronomical Society • Provided by the NASA Astrophysics Data System

1985ApJ...290..449S

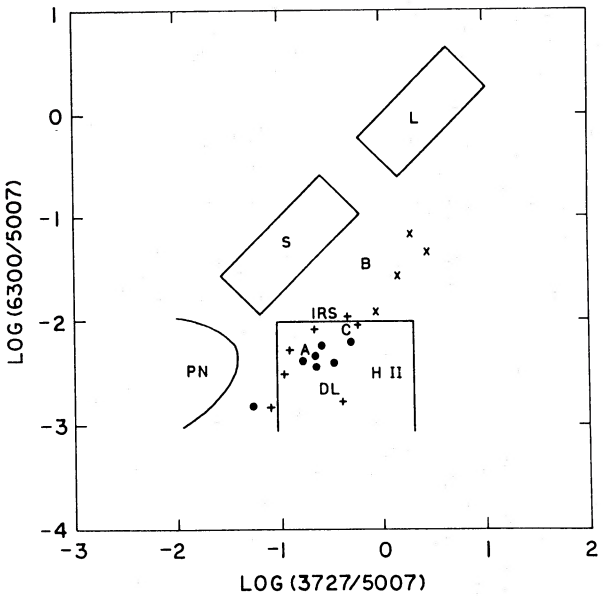

FIG. 7.—Graph of the λ6300/λ5007 ratio vs. λ3727/λ5007 for spectra at different positions in NGC 5471. Data of KS are marked with plusses (+), the low-luminosity galaxies of French with dots (·), the high-luminosity galaxies of French with crosses (×).

proposed that the winds of WR stars could be responsible for the implied supersonic motions. The blue IIDS spectra presented here represent a sensitive search for the broad emission lines of WR stars at four positions, yet no evidence of the blue emission band (4580–4730 Å) is found.

This observation can be quantified and converted to an estimate of the upper limit of the ratio of WR stars to normal early-type stars in NGC 5471. The rms deviation in the continuum was determined for each spectrum in the line-free region between 4490 and 4540 Å. At positions A, B, C, and D, the rms deviation was found to be 6%, 4%, 10%, and 9% of the continuum. Smoothing the spectra increases the sensitivity to broad features, but smoothing did not reveal any evidence of broad emission. From the rms deviations of the continuum an upper limit of 5 Å equivalent width was set for the blue WR emission band at all positions. Following the method of D'Odorico and Rosa (1981), it is assumed that WR stars have blue luminosities comparable to main sequence and supergiant O, B, and A stars. Then, adopting an equivalent width of 50 Å as the typical value for the blue emission band of a WR star places an upper limit on the fraction of WR stars at 10%. Using this method, D'Odorico and Rosa found a fraction of WR stars of 50% for NGC 604.

The emission lines of NGC 5471 are known to be broad (FWHM > 50 km s^{-1}) from both large-aperture global studies (Smith and Weedman 1970; Melnick 1977) and high-resolution slit spectra (Skillman and Balick 1984). In particular, the observations of Skillman and Balick show broad lines at the position of nucleus A, where the current observations put a strong constraint on the presence of WR stars. Since the supersonic flows produced by WR stars cannot outlive the stars, in order to account for the broad lines in terms of WR winds the proposed WR stars in NGC 5471 must have a higher efficiency of imparted mechanical energy per luminosity than the WR stars in NGC 604.

The fact that the velocity dispersion in GEHR scales with total luminosity despite a large range in fraction of luminosity contribution by WR stars argues against WR stars being the sole source of mechanical energy producing the anomalously large velocity dispersions observed. Note that this does not rule out stellar winds as a sole energy source. Abbott (1982) has shown that the total energy contribution of stellar winds from O stars can be comparable to that of WR stars when averaged over total stellar populations and lifetimes.

VI. DISCUSSION

The pioneering work of Searle (1971) demonstrated the usefulness of H II regions in studying variations in the chemical composition as a function of position in galaxies. Later theoretical work by Stasinska (1980) and French and Grandi (1981) reinforced the confidence held in abundance calculations by demonstrating that the results are, in general, independent of density inhomogeneities of the ionized gas and contributions from a mixture of exciting stars covering a range of effective temperatures. This apparent fortuitous gift of nature has been reflected in the assumptions of interpretive work. For example, RPT state that the mean squared temperature fluctuations for typical GEHRs should be ~0.01. KS dismiss observational evidence for variations in the λ3727/Hβ ratio in GEHR as attributable to calibration errors or differential refraction effects.

Such a confident stance seems unwarranted in light of what we do not understand about GEHR. The nature of the anomalously broad lines observed in GEHR is still not well understood (Gallagher and Hunter 1983; Skillman and Balick 1984). The problem of reddening estimates has already been discussed here. Since the models used to interpret the optical spectra are based on the assumption of excitation purely by photoionization, the presence of shock heating will introduce interpretive errors. Abundance analyses are sensitive to temperature estimates, which, in turn, are sensitive to reddening corrections.

The detailed study of one GEHR presented here has turned up significant variations in almost every physical characteristic studied. Perhaps most importantly, it has been shown that the presence of supernova remnants is very difficult to detect. The effects of their presence, however, are nonnegligible. NGC 5471 presents us not only with the discovery of a SNR, but also with a test case. Is there a nitrogen abundance enhancement in nucleus C, or is the increased [N II] emission due to an undetected SNR? If there is an SNR in nucleus C, then the case for common contamination of GEHR optical spectra by shock heating becomes stronger. If there is a factor of 2 nitrogen abundance difference within a single GEHR, then the studies of galactic abundance gradients based on a small number of obsevations of H II regions could be held in doubt.

In addition to the evidence for SNRs in GEHRs provided by NGC 5471, the cases of NGC 7714 and NGC 3690 should be mentioned. These two galaxies were observed by French (1980) as high-luminosity galaxies, and are found near nucleus B in Figure 7. A detailed multiwavelength study of NGC 7714 (Weedman *et al.* 1981) revealed a nonthermal radio spectrum ($\alpha = -0.6$) and an X-ray source characteristic of supernova remnants. In fact, Weedman *et al.* were led to the conclusion that NGC 7714 may contain on the order of 10^4 SNRs. Weedman *et al.* labeled NGC 7714 as the prototypical starburst nucleus. A study of NGC 3690 (Gehrz, Sramek, and Weedman 1983) also revealed a nonthermal radio component, and calculations led to an estimation of several supernovae per year. Balzano (1983) has shown that starburst nuclei form a

© American Astronomical Society • Provided by the NASA Astrophysics Data System

1985ApJ...290..449S

logical extension of the $L \propto \sigma^4$ relationship for GEHR (Terlevich and Melnick 1981). The suggestion that GEHR and starburst nuclei are members of the same class of objects and that SNRs are an important component of starburst nuclei further suggests that SNRs are important in GEHR.

Another test of the reliability of abundance determinations can be made by compiling observational results from various studies of the same object. Table 9 shows the results of calculations based on optical spectrophotometric observations of NGC 5471 taken from the literature. The temperatures derived from the [O III] lines range over almost 2000 K! Two ionic abundance ratios are compared. The O^{++}/H^+ ratio is based on the $\lambda5007 + \lambda4959/\lambda4861$ ratio and is very insensitive to reddening corrections. The He^+/H^+ ratio derived from the $\lambda5876$ line has a negligible dependence on temperature. Both ratios show significant differences from study to study. Although observational errors may account for some of these differences, it is probable that differences in aperture coverage and the method of dereddening the spectra are the primary sources of the differences noted here.

Finally, a list of questions concerning the interpretation of GEHR spectra must include a discussion of the uncertainties in the reddening correction. The best studied reddening law for an H II region (Orion) (Costero and Peimbert 1970) shows significant departures from the galactic reddening law. Since the chemical composition, gas temperature, and ionizing radiation in GEHR are quite different from those in Orion, further departures may be expected. Recently, Mathis (1983) has demonstrated how ignoring the wavelength dependence of dust albedo can lead to a misinterpretation of the Balmer decrement. There is evidence for this effect in the data presented in this paper.

Briefly, Mathis finds that the albedo of dust at Hα is larger than that at Hβ and that this leads to an underestimate of the true reddening due to dust. In Table 3, it can be seen that the values of $c(H\beta)$ derived from the Hα/Hβ ratio are generally smaller than the values of $c(H\beta)$ derived from the higher number Balmer lines, even when underlying stellar absorption is accounted for. The fact that the observed global Hα/Hβ value is less than the theoretically predicted reddening free value also supports this hypothesis. In addition, Table 9 shows that for those studies in which the reddening is based on the Hα/Hβ ratio, the reddening correction is always smaller than for those studies for which the Hα/Hβ ratio was not measured.

VII. CONCLUSIONS

From the data on NGC 5471 presented here, the following conclusions are drawn:

1. A supernova remnant has been discovered from evidence of both optical spectroscopy and radio continuum imaging. It has been shown that, although they are difficult to detect, SNRs can significantly alter the calculations of physical conditions and chemical abundances in GEHRs.
2. Differences of up to a factor of 3 have been found in the abundance of singly ionized nitrogen. If the spectra are interpreted by standard methods, there is evidence for variations of a factor of 2 in the total nitrogen abundance. It is suggested that this evidence may be explained by the presence of another, undetected SNR.
3. Differences in reddening have been found. There is evidence of both reddening by foreground clouds and internal reddening. The explanation offered by Mathis (1983) for the extinction discrepancy for GEHRs is supported by observations reported here and taken from the literature.
4. Differences in stellar populations of the exciting stars can be inferred from the observed differences in the equivalent width of Hβ at various positions.
5. The absence of any evidence of Wolf-Rayet stars must cast doubt on the theory that stellar winds from WR stars are solely responsible for the broad lines observed in GEHR.

Thanks are due to many kind people who have contributed to this paper. B. Margon and R. Downes are responsible for access to the Mount Lemmon telescope, and R. Downes assisted while collecting and reducing the Mount Lemmon data. B. Spiesman provided assistance and advice on computing problems on numerous occasions. A. Raga provided several numerical calculations from a five-level atom program. R. Sramek and D. Weedman made available B-array VLA $\lambda = 6$ cm data. Helpful input from G. Bothun is gratefully acknowledged. Numerous criticisms and suggestions by R. Kennicutt, P. Hodge, M. Goss, and the referee, R. Dufour, led to several improvements in both analysis and presentation. And finally, I would like to thank Bruce Balick, who, as thesis advisor, provided both the original ideas and continuing encouragement for this project.

The author would like to thank KPNO for the support extended to thesis students, the NRAO for support for a return trip to the VLA for data reduction, and the University of Washington Graduate School for support received in the form of a dissertation fellowship. The Mount Lemmon image-tube scanner is supported by NSF grant AST 78-09228 to UCSD.

TABLE 9

COMPARISON WITH PUBLISHED DATA

Observation[a]	Aperture	$c(H\beta)$	T(O III) (K)	O^{++}/H^+ ($\times 10^5$)	He^+/H^+ ($\lambda5876$)	Hα Used
A	4″2	0.54	12,850	9.5	0.068	no
AL	4.7	0.18	12,500	10.3	0.072	yes
IRS	22.0	0.07	13,000	7.4	0.087	yes
S + S	7	0.18	12,050	9.9	0.062	yes
S + A	2 × 4	0.10	12,900	9.7	0.065	yes
RPT	3.8 × 12.4	0.40	12,400	10.3	0.072	?
McC	4	0.25	11,450	13.7	0.077	yes
DRW	2 × 4	0.50	13,300	8.4	0.061	no

[a] S + S = Shields and Searle 1978; S + A = Sedwick and Aller 1981; RPT = Rayo, Peimbert, and Torres-Peimbert 1982; McC = McCall 1982; DRW = D'Odorico, Rosa, and Wampler 1983.

© American Astronomical Society • Provided by the NASA Astrophysics Data System

1985ApJ...290..449S

REFERENCES

Abbott, D. C. 1982, *Ap. J.*, **263**, 723.
Baldwin, J. A., Phillips, M. M., and Terlevich, R. 1981, *Pub. A.S.P.*, **93**, 5 (BPT).
Balzano, V. A. 1983, *Ap. J.*, **268**, 602.
Bignell, R. C., and Seaquist, E. R. 1983, *Ap. J.*, **270**, 140.
Brugel, E. W. 1980, Ph.D. thesis, University of Washington.
Brocklehurst, M. 1971, *M.N.R.A.S.*, **153**, 471.
———. 1972, *M.N.R.A.S.*, **157**, 211.
Butcher, H., and Oemler, A. Jr. 1978, *Astr. Ap.*, **219**, 18.
Costero, R., and Peimbert, M. 1970, *Bol. Obs. Tonantzintla y Tacubaya*, **5**, 229.
Danziger, I. J., Goss, W. M., Murdin, P., Clark, D. J., and Boksenberg, A. 1981, *M.N.R.A.S.*, **195**, 33p.
D'Odorico, S., and Dopita, M. A. 1983, in *IAU Symposium 101, Supernova Remnants and their X-ray Emission*, ed. P. Gorenstein and J. Danziger (Dordrecht: Reidel), p. 517.
D'Odorico, S., and Rosa, M. 1981, *Ap. J.*, **248**, 1015.
D'Odorico, S., Rosa, M., and Wampler, E. J. 1983, *Astr. Ap. Suppl.*, **53**, 97.
Dopita, M. A., Binette, L., D'Odorico, S., and Benvenuti, P. 1984, *Ap. J.*, **276**, 653.
Filippenko, A. V. 1982, *Pub. A.S.P.*, **94**, 715.
French, H. B. 1980, *Ap. J.*, **240**, 41.
French, H. B., and Grandi, S. A. 1981, *Ap. J.*, **244**, 493.
Gallagher, J. S., and Hunter, D. A. 1983, *Ap. J.*, **274**, 141.
Gerhz, R. D., Sramek, R. A., and Weedman, D. W. 1983, *Ap. J.*, **267**, 551.
Gilmozzi, R., Murdin, P., Clark, D. H., and Malin, D. 1983, *M.N.R.A.S.*, **202**, 927.
Hayes, D., and Massey, P. 1984, *KPNO Newsl.*, No. 33, p. 7.
Heckman, T. M. 1980, *Astr. Ap.*, **87**, 152.
Israel, F. P., Goss, W. M., and Allen, R. J. 1975, *Astr. Ap.*, **40**, 421.
Israel, F. P., and Kennicutt, R. C. 1980, *Ap. Letters*, **21**, 1.
Kennicutt, R. C. 1979, *Ap. J.*, **228**, 394.
Kunth, D., and Sargent, W. L. 1983, *Ap. J.*, **273**, 81 (KS).
Lequeux, J., Maucherat-Joubert, M., Deharveng, J. M., and Kunth, D. 1981, *Astr. Ap.*, **103**, 305.
Lequeux, J., Peimbert, M., Rayo, J. F., Serrano, A., and Torres-Peimbert, S. 1979, *Astr. Ap.*, **80**, 155.
Mathewson, D. S., and Clarke, J. N. 1973, *Ap. J.*, **189**, 725.
Mathis, J. S. 1983, *Ap. J.*, **267**, 119.
McCall, L. M. 1982, Ph. D. thesis, University of Texas.
Melnick, J. 1977, *Ap. J.*, **213**, 15.
———. 1979, *Ap. J.*, **228**, 112.
Miller, J. S. 1974, *Ap. J.*, **189**, 239.
Osterbrock, D. E. 1974, *Astrophysics of Gaseous Nebulae* (San Francisco: Freeman).
Pagel, B. E. J., Edmunds, M. G., and Smith, G. 1980, *M.N.R.A.S.*, **193**, 219.
Parker, E. A. 1968, *M.N.R.A.S.*, **138**, 407.
Peimbert, M., and Costero, R. 1969, *Bol. Obs. Tonantzintla y Tacubaya*, **5**, 3.
Pradhan, A. K. 1978, *M.N.R.A.S.*, **183**, 89p.
Rayo, J. F., Peimbert, M., and Torres-Peimbert, S. 1982, *Ap. J.*, **255**, 1 (RPT).
Rosa, M. 1980, *Astr. Ap.* **85**, L21.
Rosa, M. 1983, *Highlights Astr.*, **6**, 625.
Rubin, R. H. 1983, *Ap. J.*, **274**, 671.
Sandage, A. 1973, *Ap. J.*, **183**, 711.
Sandage, A., and Tammann, G. A. 1974*a*, *Ap. J.*, **190**, 525.
———. 1974*b*, *Ap. J.*, **194**, 223.
Schild, R. E. 1977, *A.J.*, **82**, 5.
Searle, L. 1971, *Ap. J.*, **168**, 327.
Seaton, M. J. 1975, *M.N.R.A.S.*, **170**, 475.
Sedwick, K. E., and Aller, L. H. 1981, *Proc. Nat. Acad. Sci. USA*, **78**, 1994.
Seyfert, C. K. 1940, *Ap. J.*, **91**, 261.
Shields, G. A., and Searle, L. 1978, *Ap. J.*, **222**, 821.
Shields, G. A., and Tinsley, B. M. 1976, *Ap. J.*, **203**, 66.
Skillman, E. D. 1984, Ph. D. thesis, University of Washington.
Skillman, E. D., and Balick, B. 1984, *Ap. J.*, **280**, 580.
Smith, M. G., and Weedman, D. W. 1970, *Ap. J.*, **161**, 33.
———. 1972, *Ap. J.*, **172**, 307.
Stasinska, G. 1980, *Astr. Ap.*, **84**, 320.
Terlevich, R., and Melnick, J. 1981, *M.N.R.A.S.*, **195**, 839.
Tody, D. 1980, *Proc. SPIE*, **264**, 121.
Tully, R. B., Boesgaard, A. M., Dyck, H. M., and Schempp, W. V. 1981, *Ap. J.*, **246**, 38.
Viallefond, F., Allen, R. J., and Goss, W. M. 1981, *Astr. Ap.*, **104**, 127 (VAG).
Weedman, D. W., Feldman, F. R., Balzano, V. A., Ramsey, L. W., Sramek, R. A., and Wu, C. 1981, *Ap. J.*, **248**, 105.
Whitford, A. E. 1958, *A.J.*, **63**, 210.

EVAN D. SKILLMAN: Astronomy Department, FM-20, University of Washington, Seattle, WA 98195

© American Astronomical Society • Provided by the NASA Astrophysics Data System